Nanoscale Advances

ROYAL SOCIETY OF CHEMISTRY

PAPER

View Article Online
View Journal | View Issue

Cite this: *Nanoscale Adv.*, 2024, **6**, 3135

Enhancing anti-angiogenic immunotherapy for melanoma through injectable metal–organic framework hydrogel co-delivery of combretastatin A4 and poly(I:C)

Xufeng Xiao,†[a] Yunuo Zheng,†[d] Tianlong Wang,[a] Xiaoqing Zhang,[a] Gaochuan Fang,[a] Zhonghai Zhang,[a] Zhengkui Zhang*[bc] and Jiaojiao Zhao *[a]

The interplay between vascularization and macrophage-induced immune suppression plays a crucial role in melanoma treatment. In this study, we propose a novel combination approach to combat melanoma by simultaneously inhibiting tumor vascularization and enhancing macrophage-mediated anti-tumor responses. We investigate the potential of combining combretastatin A4 (CA4), a vascular-disrupting agent, with poly(I:C) (PIC), an immunostimulatory adjuvant. This combination approach effectively suppresses melanoma cell proliferation, disrupts vascularization, and promotes macrophage polarization towards the M1 phenotype for melanoma suppression. To facilitate efficient co-delivery of CA4 and PIC for enhanced anti-angiogenic immunotherapy, we develop an injectable metal–organic framework hydrogel using Zeolitic Imidazolate Framework-8 (ZIF-8) and hyaluronic acid (HA) (ZIF-8/HA). Our findings demonstrate that ZIF-8 enables efficient loading of CA4 and enhances the stability of PIC against RNAase degradation *in vitro*. Furthermore, the developed co-delivery hydrogel system, PIC/CA4@ZIF-8/HA, exhibits improved rheological properties, good injectability and prolonged drug retention. Importantly, *in vivo* experiments demonstrate that the PIC/CA4@ZIF-8/HA formulation significantly reduces the dosage and administration frequency while achieving a more pronounced therapeutic effect. It effectively inhibits melanoma growth by suppressing angiogenesis, destroying blood vessels, promoting M1 macrophage infiltration, and demonstrating excellent biocompatibility. In conclusion, our study advances anti-angiogenic immunotherapy for melanoma through the potent combination of PIC/CA4, particularly when administered using the PIC/CA4@ZIF-8/HA formulation. These findings provide a new perspective on clinical anti-angiogenic immunotherapy for melanoma, emphasizing the importance of targeting tumor vascularization and macrophage-mediated immune suppression simultaneously.

Received 26th January 2024
Accepted 29th April 2024

DOI: 10.1039/d4na00079j

rsc.li/nanoscale-advances

1. Introduction

Melanoma, a highly aggressive form of cutaneous malignancy, remains a significant cause of cancer-related mortality worldwide.[1] Despite advancements in therapeutic strategies, the prognosis for patients with advanced melanoma remains unfavorable.[2] T cell-based immune checkpoint inhibitors have shown promise in clinical management, but challenges such as limited response rates, drug resistance, and systemic toxicity still persist.[3,4] Therefore, there is an urgent need to explore combination therapies that can enhance the effectiveness of immunotherapy.[5]

Macrophages, as versatile innate immune cells, play a critical role in tumor development by infiltrating tumor tissues and giving rise to tumor-associated macrophages (TAMs).[6] TAMs can be classified into two main subtypes: anti-tumor M1 TAMs and pro-tumor M2 TAMs.[7] Infiltration of M2 TAMs into primary melanoma lesions promotes angiogenesis, facilitating tumor invasion and metastasis.[8] Moreover, macrophages contribute to the formation of vascular mimicry channels, further aiding tumor progression.[9] Importantly, M2 TAMs-mediated angiogenesis limits the effectiveness of immune checkpoint inhibitor therapy.[10] Therefore, combining anti-angiogenesis and immune-boosting therapies is a promising approach for

[a]*Jiangsu Key Laboratory of Phylogenomics and Comparative Genomics, Jiangsu International Joint Center of Genomics, School of Life Sciences, Jiangsu Normal University, Xuzhou, 221116, Jiangsu, China. E-mail: jiaojiaozhao@jsnu.edu.cn*

[b]*Institute of Nervous System Diseases, Xuzhou Medical University, Xuzhou, 221002, Jiangsu, China. E-mail: zkzhang@xzhmu.edu.cn*

[c]*Department of Neurosurgery, Affiliated Hospital of Xuzhou Medical University, Xuzhou, 221002, Jiangsu, China*

[d]*Department of Obstetrics and Gynecology, Xuzhou Central Hospital, Xuzhou, 221009, Jiangsu, China*

† These authors contributed equally to this work.

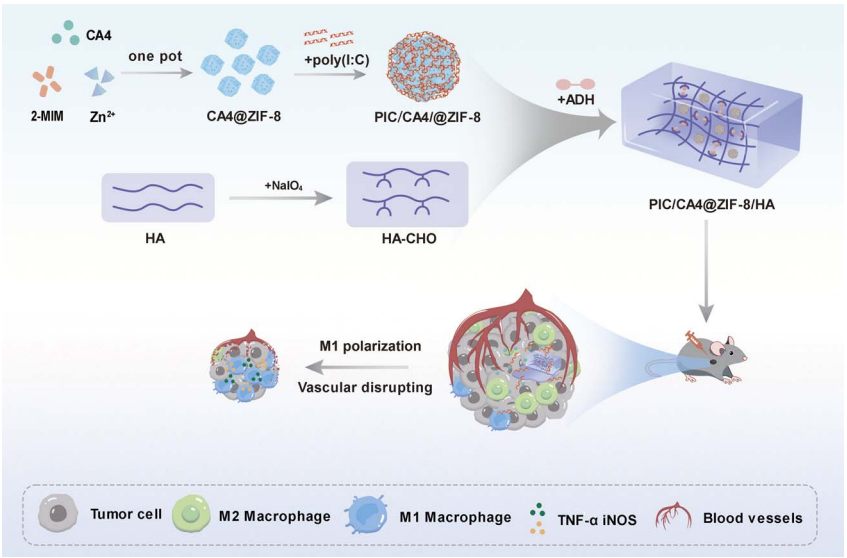

Scheme 1 An enhanced anti-angiogenic immunotherapy therapeutic effect of melanoma through PIC/CA4@ZIF-8/HA.

melanoma treatment.[11] Previous studies conducted by our research team and other scholars have demonstrated that the reprogramming of M2 TAMs into M1 TAMs can effectively remodel the tumor microenvironment and inhibit angiogenesis.[12,13] However, it is crucial to note that alternative mechanisms of angiogenesis may counteract the effects of these anti-angiogenic treatments.[14] In response to this challenge, the use of vascular-disrupting agents has emerged as a promising strategy. These agents induce a rapid shutdown and collapse of tumor blood vessels, leading to ischemia and subsequent necrosis of the tumor mass.[15] This therapeutic modality has proven to be of significant importance in enhancing tumor suppression and promoting an immune response.[16,17] Building on these discoveries, we propose a combined treatment approach that involves reprogramming macrophages and disrupting tumor vasculature for a synergistic therapeutic effect.

Poly(I:C) (PIC) is a synthetic double-stranded RNA molecule that has the ability to induce innate immune responses, particularly in the modulation of TAMs towards an anti-tumor M1 phenotype.[18–20] Combretastatin A4 (CA4), a potent vascular-disrupting agent, has demonstrated potential in preclinical trials by selectively targeting and eliminating tumor blood vessels.[21,22] However, the presence of M2 TAMs in the tumor microenvironment limits the therapeutic efficacy of CA4.[23] Therefore, we propose a combined approach using PIC and CA4 to achieve a synergistic therapeutic outcome. PIC can reprogram macrophages towards an M1 polarization, resulting in a positive immune response, inhibition of angiogenesis, and enhanced therapeutic efficacy of CA4. Simultaneously, CA4 can disrupt tumor vasculature, counteracting alternative angiogenic mechanisms. This integrated approach holds great potential for improving melanoma treatment outcomes. Nevertheless, efficient delivery of both PIC and CA4 to the tumor site, which is crucial for enhanced therapeutic efficacy, presents challenges. PIC is susceptible to enzymatic degradation, while CA4 requires specific targeting and accumulation in tumor tissues for optimal biosecurity. To overcome these obstacles and maximize the therapeutic potential of the combined treatment approach, the development of an efficient drug delivery system is imperative.

Metal–organic frameworks (MOFs) have emerged as versatile platforms for drug delivery due to their adjustable characteristics, high drug-loading capacity, and biocompatibility.[24,25] Injectable MOF hydrogels, which are composite materials comprising MOFs and polymeric hydrogels, have gained significant attention for their *in situ* injectability, allowing localized and sustained drug delivery.[26] Zeolitic Imidazolate Framework-8 (ZIF-8) is a promising MOF material known for its stability, porous structure, and large surface area.[27] ZIF-8 has been extensively explored as a nanocarrier for siRNA, protecting it from enzymatic degradation and enabling targeted delivery to the tumor site.[28,29] Integration of ZIF-8 into hydrogel compositions offers improved mechanical strength, stability, and controlled release of drugs or biologically active compounds.[30] Additionally, ZIF-8 has been successfully employed in a GelMA-Z hydrogel that can be injected, demonstrating its biocompatibility and improved therapeutic efficacy.[31] It is worth noting that the sustained release of drug-loaded nanoparticles from injectable hydrogels has demonstrated promise in manipulating macrophage phenotype and advancing immune-regenerative medicine.[32] Based on this background, our objective was to develop an injectable ZIF-8 hydrogel system capable of co-delivering CA4 and PIC to enhance anti-vascular immunotherapy for melanoma.

In this study, we have demonstrated the synergistic effect of the PIC/CA4 combination in anti-angiogenic immunotherapy for melanoma. Additionally, we have successfully developed the injectable PIC/CA4@ZIF-8/HA system, which effectively protects PIC from enzymatic degradation and enables controlled release of both PIC and CA4 within the tumor tissue. Consequently, we

observed more pronounced effects in anti-angiogenic immunotherapy, where the PIC/CA4@ZIF-8/HA formulation significantly suppressed angiogenesis, induced blood vessel destruction, and promoted infiltration of M1 macrophages (Scheme 1). These innovative advancements not only provide important insights into the intricate interplay among angiogenesis, vascularization, and immune suppression in melanoma but also offer valuable prospects for the development of novel treatment strategies.

2. Materials and methods

2.1. Materials

Hyaluronic acid (HA), sodium periodate ($NaIO_4$), and adipic dihydrazide (ADH) were obtained from Shanghai Innochem Scientific Co., Ltd. Poly(I:C) was acquired from InvivoGen Co., Ltd. Trizol reagent, HiScript® II Q RT SuperMix, and SYBR Green PCR Mix were purchased from Vazyme Biotech Co., Ltd. RNAase was purchased from Beyotime Co., Ltd. Dulbecco's Modified Eagle Medium (DMEM) with 10% fetal bovine serum (FBS) and 1% v/v penicillin/streptomycin was obtained from Wisent. Endothelial cell medium (ECM) complete medium, containing 5% FBS, 1% v/v penicillin/streptomycin, and 1% endothelial cell growth supplement, was obtained from ScienCell. Mouse melanoma cells B16F10 and macrophage cells RAW264.7 were obtained from the Shanghai Cell Bank of the Chinese Academy of Science. Collagenase was acquired from Sigma-Aldrich. Matrigel was sourced from BD Biosciences. The DyLight™ 594 Lycopersicon Esculentum Lectin was obtained from Vector Labs. The F4/80 and CD86 antibodies were purchased from Novus Biologicals and Bio-Rad, respectively.

2.2. Cells and cell culture

Human umbilical vein endothelial cells (HUVECs) were isolated from fresh umbilical cords in accordance with the ethical guidelines stated in the Declaration of Helsinki and approved by the Xuzhou Central Hospital Ethics Committee. Neonatal umbilical cords obtained within 4 hours of separation were clamped using hemostatic forceps. Subsequently, the cord was injected with preheated 0.1% collagenase and subjected to digestion at 37 °C for 10 minutes. Following digestion, the umbilical cord was rinsed twice with PBS to isolate the cells. The isolated cells were then centrifuged at 1000 rpm for 10 minutes and washed again with PBS. Finally, the HUVECs were cultured in preheated ECM complete medium and maintained for up to six generations for the purpose of this study. Both melanoma and macrophage cells were cultured in DMEM supplemented with 10% FBS and 1% v/v penicillin–streptomycin. All cells were maintained in a humidified incubator at 37 °C with 5% CO_2.

2.3. Tube formation assay

The matrigel was thawed overnight on ice. Then, each well of a 96-well plate was coated with 100 μL of pre-chilled matrigel. The plate was incubated at 37 °C for 30 minutes to allow the matrigel to solidify. HUVEC cells were divided into four groups and treated with PBS, PIC, CA4, and PIC/CA4, respectively. Subsequently, each group of HUVEC cells was seeded onto the matrigel-coated wells and incubated at 37 °C for 6 hours. The formation of capillary-like tubes was observed using a phase-contrast microscope (Olympus, Tokyo, Japan).

2.4. Quantitative real-time PCR (qRT-PCR) assay

To assess gene expression levels, total ribonucleic acid (RNA) was isolated from RAW264.7 cells using Trizol Reagent, following the manufacturer's protocol. Subsequently, the extracted RNA was reverse-transcribed into complementary DNA using the HiScript® II Q RT SuperMix. The primer sequences used in this study can be found in Table 1, and the SYBR Green PCR Mix was used according to the kit instructions. PCR reactions were carried out using the LightCycler 96 instrument (Roche, Basel, Switzerland). Finally, the relative expression of the target genes was determined using the $2^{-\Delta\Delta Ct}$ method.

2.5. Synthesis and characterization of CA4@ZIF-8 and PIC/CA4@ZIF-8

The synthesis of CA4@ZIF-8 was conducted using a one-pot method. Precise amounts of zinc nitrate hexahydrate, 2-methylimidazole, and CA4 were individually dissolved in methanol. The CA4 solution was then combined with zinc nitrate hexahydrate and stirred at 1700 rpm at 0 °C. Afterwards, the 2-methylimidazole was added to the mixture, and stirring continued for approximately 25 minutes. The resulting suspension was centrifuged at 10 000 rpm and 4 °C for 10 minutes to remove the methanol. The precipitate was washed three times with methanol to obtain the CA4@ZIF-8 nanoparticles. The drug loading capacity of CA4@ZIF-8 was determined using a UV-vis spectrophotometer (Shimadzu UV-2501PC, Japan). To synthesize PIC/CA4@ZIF-8, electrostatic adsorption was employed. Specifically, the obtained ZIF-8 and PIC were mixed in various mass ratios and subjected to agarose gel electrophoresis. The successful incorporation of PIC into ZIF-8 was determined by observing the retardation of PIC in the gel wells. Subsequently, the hydrodynamic diameter and zeta potential of CA4@ZIF-8 and PIC/CA4@ZIF-8 were measured

Table 1 Primer sequences for real-time RT-PCR analysis

Gene	Forward	Reverse
GAPDH	TGGCCTTCCGTGTTCCTAC	GAGTTGCTGTTGAAGTCGCA
TNF-α	CCCTCACACTCAGATCATCTTCT	GCTACGACGTGGGCTACAG
iNOS	GGAGTGACGGCAAACATGACT	TCGATGCACAACTGGGTGAAC

using Dynamic Light Scattering (DLS) with the Zetasizer Nano ZS ZEN3600 instrument (Malvern, UK).

2.6. Synthesis and characterization of PIC/CA4@ZIF-8/HA

Sodium periodate ($NaIO_4$) was used to oxidize HA, resulting in oxidized aldehyde hyaluronic acid (HA-CHO). The chemical structure of HA-CHO was then examined using Fourier transform infrared spectroscopy (FTIR) with a Thermo Scientific Nicolet iS5 instrument (Waltham, MA, USA). To create a water gel that encapsulates PIC/CA4@ZIF-8, a one-pot method was employed. Initially, a 4% aqueous solution of HA-CHO was prepared by dissolving an appropriate amount of HA-CHO. Subsequently, ADH was added to the solution containing PIC/CA4@ZIF-8. The mixture solution was then added to the HA-CHO aqueous solution. The successful gelation of the water gel was evaluated using the tilted tube test, where gelation was confirmed if no significant flow was observed within 1 minute. Furthermore, the rheological properties of HA and PIC/CA4@ZIF-8/HA hydrogel were assessed using a rotational rheometer (MCR 302, Anton Paar, Austria) with a constant strain of 1% and a frequency range from 0.1 Hz to 100 Hz. The gel morphology was characterized using a scanning electron microscope (SEM) (SU8010, Hitachi, Japan).

2.7. PIC protection assay

To assess the protective effect of PIC-containing ZIF-8 formulations (PIC@ZIF-8) against RNAase, an electrophoretic mobility assay was conducted. The PIC@ZIF-8 nanoparticles were incubated with RNAase at 37 °C for different durations (0, 1, 3, 6, and 12 hours), with free PIC serving as the control. Afterwards, the PIC@ZIF-8 nanoparticles were acidulated using a hydrochloric acid solution. A portion of each sample was collected and subjected to gel electrophoresis on a 1% agarose gel in Tris–acetate–EDTA buffer at 90 V for 30 minutes. Subsequently, the gel was stained with gel red, and images were captured using a gel documentation system (ChampGe16000, China).

2.8. *In vivo* retention of gel

Indocyanine green (ICG),[33] a highly luminescent fluorescent dye with exceptional properties, was chosen as a substitute for CA4 and PIC to mimic their retention and distribution *in vivo*. This approach allowed us to assess the retention capability of the hydrogel towards the encapsulated nanoparticles. The ICG-loaded ZIF-8 (ICG@ZIF-8) and ICG-loaded ZIF-8 hydrogel (ICG@ZIF-8/HA) were prepared using a method similar to that used for CA4@ZIF-8 and CA4@ZIF-8/HA. For *in vivo* fluorescence imaging, a subcutaneous injection of 100 μL of free ICG, ICG@ZIF-8, and ICG@ZIF-8/HA was administered to C57BL/6 mice. The fluorescence signals were monitored at specified time points using an AniView100 system (BLT, Guangzhou, China).

2.9. Animal model and *in vivo* therapy

Female C57BL/6 mice aged 6–8 weeks were sourced from the Laboratory Animal Center of Xuzhou Medical University, Jiangsu, China. All animal procedures and protocols in this study strictly followed the ethical standards established by Xuzhou Medical University for animal studies (No. 202104A015). To establish a subcutaneous melanoma model, we subcutaneously injected 5×10^5 B16F10 cells suspended in 100 μL of PBS into the right armpit of each mouse. After one week, the mice were randomly divided into four groups, each containing six mice. For the combination drug experiment, the following four groups were established: PBS, CA4, PIC, and PIC/CA4. The objective was to evaluate the potential synergistic therapeutic effect between CA4 and PIC. Additionally, for the drug co-delivery experiment, we created four groups: PBS, PIC/CA4, PIC/CA4@ZIF-8, and PIC/CA4@ZIF-8/HA. The aim of this experiment was to assess whether the ZIF-8/HA delivery system could significantly enhance treatment efficacy. It is important to note that the injection volume for each group was maintained at 100 μL to ensure consistency across experimental conditions. Subsequently, the maximum tumor length (L) and minimum tumor width (W) were measured every two days. The tumor volume (V) was calculated using the formula: $V = (L \times W^2)/2$. At the end of the study, all mice were euthanized. Tumor tissues were dissected, weighed, photographed and subjected to immunohistochemical staining. Furthermore, the heart, liver, spleen, lungs, and kidneys were collected for safety evaluation.

2.10. Histologic analysis of tumor vessels

The changes in tumor vessels were evaluated using an intravascular perfusion method. Prior to euthanizing the mice, each mouse received an intravenous injection of DyLight™ 594 Lycopersicon Esculentum Lectin at a volume of 100 μL (1 mg mL^{-1}) through the tail vein. After a five-minute interval, the mice were euthanized, and tumor tissues were collected for the preparation of frozen slices. The frozen slices were then stained with 2-(4-amidinophenyl)-6-indolecarbamidine dihydrochloride to counterstain the nuclei. Finally, the frozen slices were imaged using a laser scanning confocal microscope (Andor Technology PLC, Belfast, Ireland).

2.11. Immunohistochemistry

Immunohistochemical staining was performed using a two-step immunocytochemistry protocol. Tumor tissue samples were fixed in 4% paraformaldehyde, embedded in paraffin, and sectioned to a thickness of 5 μm. To enhance immunoreactivity, the sections underwent a 10 minute treatment with citrate buffer (pH 6.0). Subsequently, bovine serum albumin was applied to the sections and incubated for 30 minutes to block nonspecific staining. Primary antibodies, F4/80 and CD86, were separately added to the sections and allowed to incubate overnight at 4 °C. Following the overnight incubation, the sections were treated with a peroxidase-labeled goat anti-mouse IgG secondary antibody. After washing with PBS, the sections were stained with DAB and counterstained with hematoxylin. Finally, the slides were examined using CaseViewer (3DHISTECH Ltd., Budapest, Hungary).

2.12. Statistical analysis

Data analysis was conducted using GraphPad Prism (GraphPad Inc.). The results were represented as means ± standard deviation. Statistical analysis was performed using a one-way ANOVA for comparisons among multiple groups. The significance of the difference was indicated by comparing them to the corresponding controls (*$P < 0.05$, **$P < 0.01$, ***$P < 0.001$, or ****$P < 0.0001$).

3. Results and discussion

3.1. The impact of PIC/CA4 on cell viability, tube formation, and macrophage polarization

The anti-tumor efficacy of CA4 has been established through its direct suppression of tumor cell proliferation and disruption of tumor blood vessels.[34] To assess the impact of CA4 on B16F10 cell viability, a CCK-8 cell viability assay was conducted using various concentrations of CA4. As shown in Fig. 1A, a dose-dependent inhibition of B16F10 cell viability by CA4 was observed. At concentrations of 0.2 or 1 nM, CA4 resulted in less than 20% inhibition of cell viability. However, at 5 nM, approximately 40% of B16F10 cell viability was inhibited. Further increasing the concentration to 25 or 125 nM did not result in a significant difference in inhibition compared to 5 nM. Based on these findings, 5 nM CA4 was selected for further investigations. To explore the combined effect of CA4 and PIC on B16F10 cell viability, a concentration of 10 μg mL^{-1} of PIC, which has been demonstrated to activate macrophages in our previous work,[19] was chosen. As depicted in Fig. 1B, the combination of PIC/CA4 exhibited a stronger impact on B16F10 cell viability compared to either treatment alone. CA4 alone inhibited approximately 40% of cell viability, while PIC treatment alone showed only around 10% inhibition. However, the combination of CA4 and PIC significantly suppressed over 50% of B16F10 cell viability, surpassing the inhibitory effects of CA4 or PIC alone. These findings indicate a synergistic inhibition of B16F10 cell viability by PIC/CA4.

HUVEC cells are commonly employed as a cellular model for studying angiogenesis.[35] Considering the significance of cell viability in angiogenesis, we conducted CCK-8 cell viability assays to evaluate the effects of CA4, PIC, and PIC/CA4 on HUVEC cell viability. The results, presented in Fig. 1C, indicated that both CA4 and PIC individually exerted inhibitory effects on HUVEC cell viability, with CA4 inhibiting approximately 80% and PIC inhibiting approximately 56% of cell viability. In contrast, the combination of PIC/CA4 demonstrated a more pronounced effect, suppressing over 85% of HUVEC cell viability. Furthermore, a tube formation assay was conducted to examine the effects of CA4, PIC, and PIC/CA4 on the tube-forming ability of HUVEC cells. The control group exhibited well-defined and intact tube structures with multiple nodules (Fig. 1D). The PIC treatment group displayed a reduction in tube formation compared to the control group, characterized by relatively fewer and incomplete nodules, indicating its inhibitory effect on HUVEC tube formation. The CA4 treatment group exhibited a distinct absence of vascular-like structures, indicating a significant disruption of HUVEC tube formation by CA4. In the PIC/CA4 treatment group, no noticeable distinction was observed compared to the CA4 group, suggesting that the inhibitory effect of PIC/CA4 on HUVEC tube formation is primarily attributed to CA4.

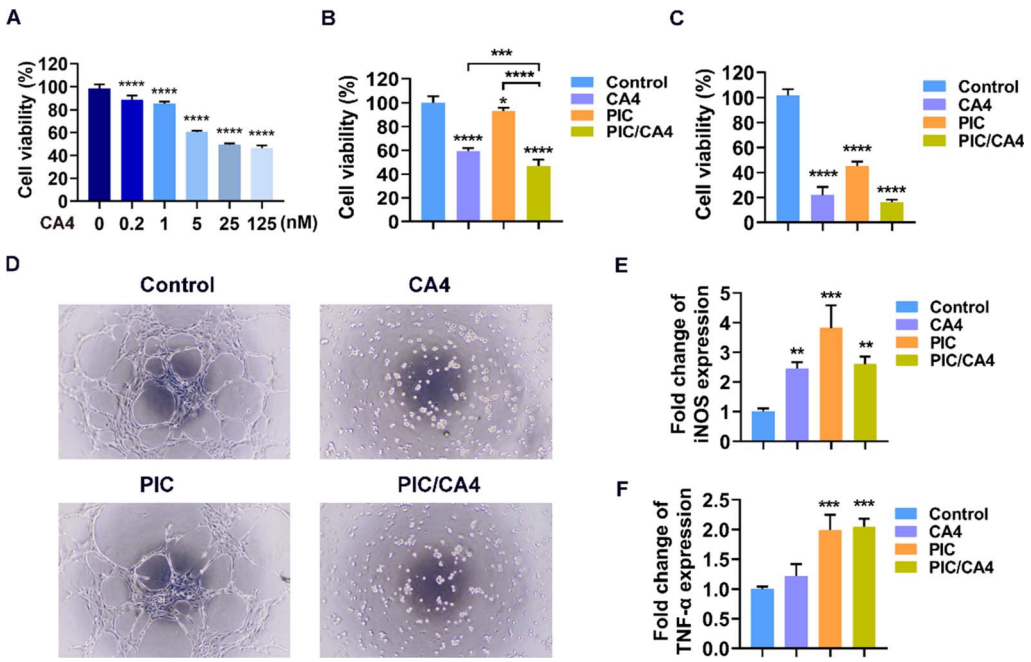

Fig. 1 The impact of PIC/CA4 on cell viability, tube formation, and macrophage polarization. (A and B) The cell viability of B16F10 cells. (C) The cell viability of HUVEC cells. (D) The impact of CA4, PIC, and PIC/CA4 on the tube formation of HUVEC cells. The impact of CA4, PIC, and PIC/CA4 on the expression of iNOS (E), and TNF-α (F) in RAW 264.7 cells.

To further investigate the effects of CA4, PIC, and PIC/CA4 on macrophage polarization *in vitro*, qRT-PCR experiments were performed to evaluate changes in the expression of M1 marker genes, namely iNOS and TNF-α in RAW264.7 cells.[36] The results demonstrated that the iNOS gene was significantly upregulated in all treatment groups (CA4, PIC, and PIC/CA4) compared to the control group (Fig. 1E). Additionally, except for CA4, both PIC and PIC/CA4 treatments led to a significant increase in TNF-α expression (Fig. 1F). In summary, the use of PIC/CA4 exhibited significant effectiveness in inhibiting melanoma cell proliferation, disrupting tube formation, and promoting the polarization of macrophages towards the M1 phenotype.

3.2. PIC/CA4 synergistically suppresses melanoma growth in mice

To investigate the effects of combined PIC/CA4 treatment on mouse melanoma growth, we divided tumor-bearing mice into different treatment groups: PBS, CA4 (10 mg kg^{-1}), PIC (1 mg kg^{-1}), and PIC/CA4 (1 mg kg^{-1}/10 mg kg^{-1}). The treatments were administered every other day for a total of three treatments (Fig. 2A). The results demonstrated that treatment with CA4 alone did not effectively suppress tumor growth, indicating that the mere disruption of blood vessels may not be sufficient for effective tumor suppression (Fig. 2B and C). In contrast, treatment with PIC alone showed a significant inhibition of tumor growth, consistent with our previous study.[19] Importantly, the combination of PIC/CA4 exhibited a more pronounced inhibitory effect on melanoma growth compared to CA4 or PIC alone, indicating a synergistic effect of PIC and CA4 in tumor suppression. These findings suggest that the simultaneous promotion of macrophage immune activation and the disruption of blood vessels can effectively inhibit tumor progression.

Histopathological examination of tumor tissues using H&E staining revealed a higher tumor cell density with closely packed cells in the control, CA4, and PIC treatment groups. In contrast, the PIC/CA4 treatment group displayed a significant reduction in the number of tumor cells, which were loosely arranged (Fig. 2D), indicating a synergistic inhibition of melanoma cell proliferation *in vivo* by PIC/CA4. Furthermore, the control group exhibited numerous irregular and enlarged blood vessels within the tumor tissues, while all the treatment groups, including CA4, PIC alone, and PIC/CA4, exhibited a substantial reduction in tumor vasculature. Additionally, histological examination using H&E staining revealed the infiltration of immune cells in the tumor tissues across various groups. Notably, the PIC/CA4 treatment group exhibited the most pronounced level of immune cell infiltration compared to the control, CA4, and PIC treatment groups. This suggests that the combined administration of PIC/CA4 synergistically enhances the recruitment of immune cells, thereby facilitating tumor suppression.

To further evaluate the impact of different treatment modalities on tumor vasculature, we employed tomato lectin to label blood vessels in tumor tissues and examined vascular alterations among the various treatment groups. The results presented in Fig. 2E demonstrate the presence of red-labeled

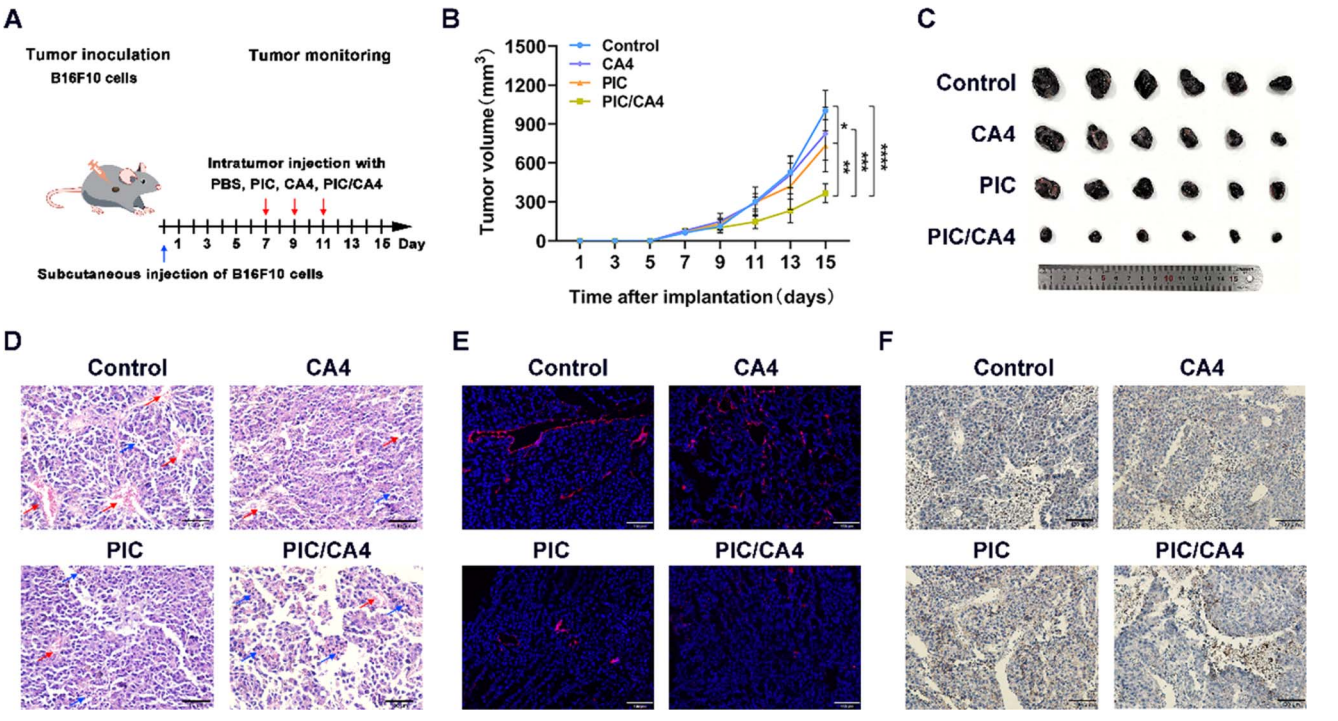

Fig. 2 PIC/CA4 synergistically suppresses melanoma growth in mice. (A) Schematic diagram of tumor-bearing mice treatment. The growth curves (B) and representative tumor tissues (C) of mouse tumors treated with PBS, CA4, PIC, and PIC/CA4. (D) H&E staining images of tumor tissue treated with PBS, CA4, PIC, and PIC/CA4. Red arrows indicate the vascular tissues and the blue arrows indicate immune cells. Scale bar, 100 μm. (E) Representative images of tumor vessel density in tumor tissues. Scale bar, 100 μm. (F) Immunohistochemical staining of CD86 expression in mouse tumor tissue. Scale bar, 100 μm.

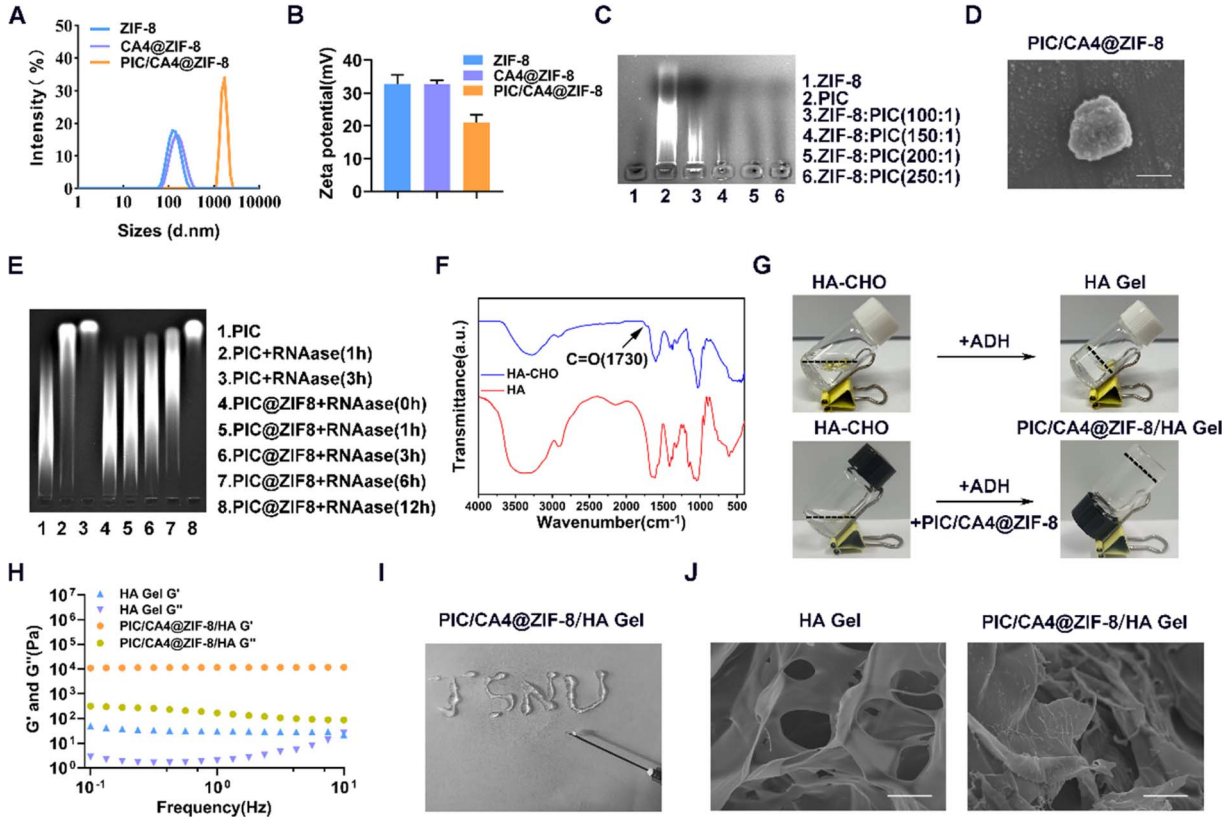

Fig. 3 Characterization of the PIC/CA4@ZIF-8 and PIC/CA4@ZIF-8/HA. Hydrated particle sizes (A) and zeta potentials (B) of ZIF-8, CA4@ZIF-8 and PIC/CA4@ZIF-8. (C) Gel electrophoresis results of ZIF-8 and PIC mixed at different mass ratios. (D) Representative SEM image of PIC/CA4@ZIF-8. Scale bar: 500 nm. (E) Agarose gel electrophoretogram showing the protection of PIC by ZIF-8 during incubation, compared to naked PIC. (F) The FTIR image of HA and HA-CHO. (G) Macrographs of HA and PIC/CA4@ZIF-8/HA with addition of ADH to form Gels. (H) Dynamic frequency sweep of the HA gel and PIC/CA4@ZIF-8/HA gel. (I) Photograph of the injectability of PIC/CA4@ZIF-8/HA gel. (J) Representative SEM image of HA and PIC/CA4@ZIF-8/HA gels. Scale bar: 5 μm.

blood vessels within the tumor tissues. Consistent with the H&E staining results, the control group exhibited large and intact blood vessels, forming irregular circular patterns. In contrast, the CA4 treatment group displayed significantly disrupted blood vessels with fragmentation and a dense distribution. This suggests that CA4 specifically targets and eliminates pre-existing tumor blood vessels without affecting the process of angiogenesis. In the PIC treatment group, there was a noticeable suppression of blood vessel formation accompanied by a reduction in vessel lumen size. Remarkably, the PIC/CA4 combination group exhibited the most pronounced effect on tumor vasculature, with minimal fragmentation observed. This suggests that the synergistic action of PIC and CA4 effectively inhibits angiogenesis and disrupts tumor blood vessels in melanoma.

Previous research has demonstrated a strong association between macrophage infiltration and angiogenesis, where M2 macrophages promote angiogenesis while M1 macrophages inhibit it.[37] To investigate the influence of PIC/CA4 treatment on M1 macrophage infiltration in tumor tissues, we performed immunocytochemistry to evaluate the protein expression of the M1 macrophage marker CD86. The results depicted in Fig. 2F show a significant increase in the number of M1 macrophages in the tumor tissues of the PIC and PIC/CA4 treatment groups compared to the control and CA4 treatment group, suggesting that the infiltration of M1 macrophages plays a crucial role in suppressing tumor growth. Importantly, considering the combined results from Fig. 2B and C, it is evident that PIC/CA4 treatment has a more significant therapeutic effect than PIC alone, indicating that the simultaneous promotion of M1 macrophage infiltration and disruption of tumor tissue vascularization leads to a greater therapeutic outcome.

3.3. Characterization of the PIC/CA4@ZIF-8 and PIC/CA4@ZIF-8/HA

Despite the potential advantages of combining PIC and CA4, there are still several challenges that need to be addressed, including high dosage requirements, frequent administration, lack of targeted delivery, and uncontrolled release. To overcome these challenges, we propose the utilization of MOF hydrogels composed of ZIF-8 and HA, referred to as ZIF-8/HA. These composite materials possess adjustable structures and exhibit the drug-loading capabilities of ZIF-8, as well as the biocompatibility, targeted administration, and controlled drug release characteristics of HA hydrogels.[26] Therefore, our hypothesis is that co-delivery of PIC and CA4 using ZIF-8 can effectively

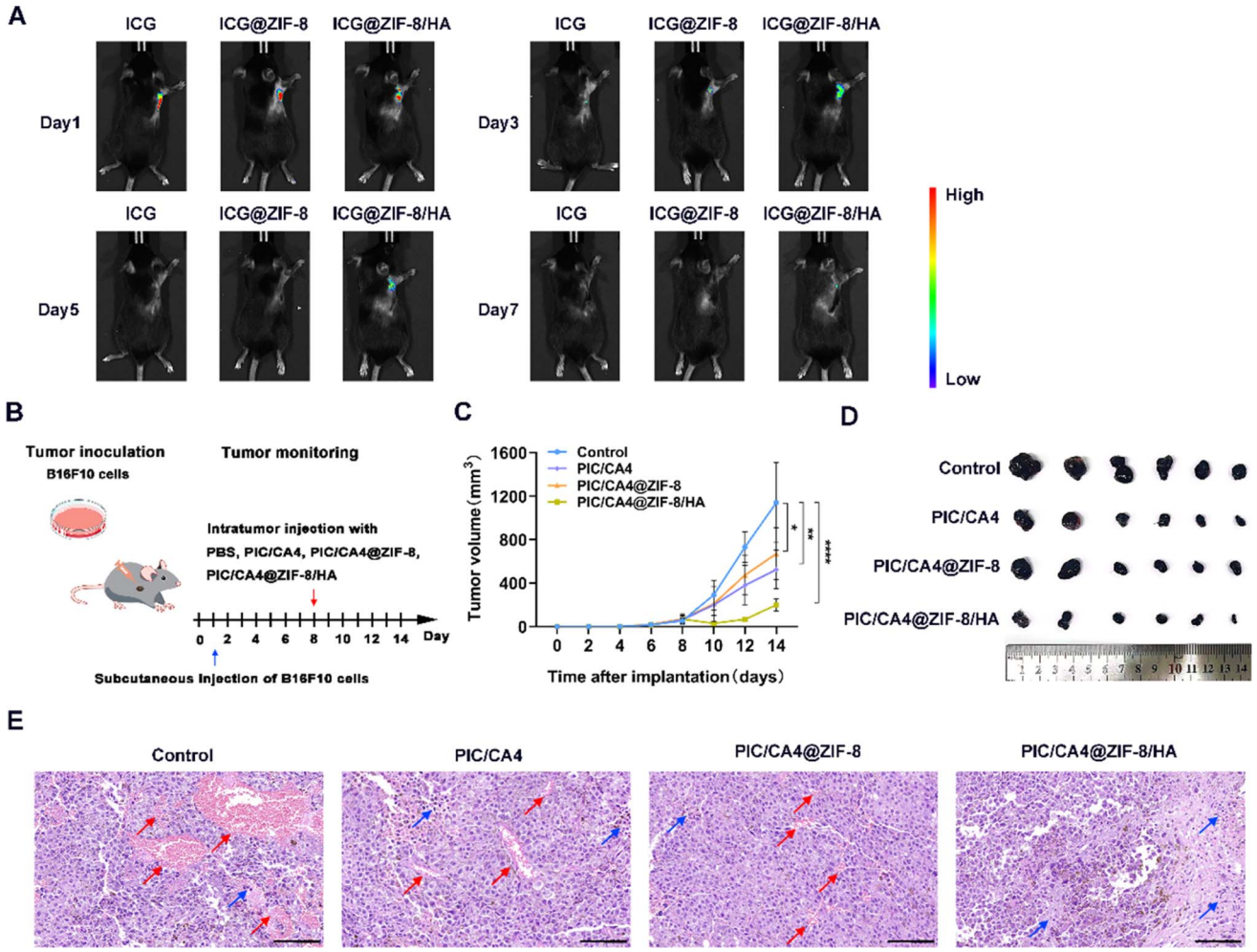

Fig. 4 PIC/CA4@ZIF-8/HA exhibits a more pronounced therapeutic effect in melanoma. (A) Fluorescence IVIS images of mice injected with free ICG, ICG@ZIF8, and ICG@ZIF8/HA. (B) Schematic diagram of tumor-bearing mice treatment. The growth curves (C) and representative tumor tissues (D) of mouse tumors treated with PBS, PIC/CA4, PIC/CA4@ZIF-8 and PIC/CA4@ZIF-8/HA. (E) H&E staining images of tumor tissue treated with PBS, PIC/CA4, PIC/CA4@ZIF-8 and PIC/CA4@ZIF-8/HA. Red arrows indicate the vascular tissues and the blue arrows indicate immune cells. Scale bar, 100 μm.

protect the drugs from enzymatic degradation or rapid clearance. Furthermore, the injectability and drug-releasing properties of ZIF-8/HA can allow for single-dose administration, dose reduction, and precise drug release within tumor tissues, thereby enhancing the efficacy and safety of melanoma treatment.

We synthesized ZIF-8 and CA4@ZIF-8 nanomaterials using a one-pot synthesis method. The loading capacity of ZIF-8 for CA4 was confirmed to be approximately 8.6% through UV absorption spectroscopy. The hydrodynamic diameter of CA4@ZIF-8 was measured to be 148 ± 1 nm, with a zeta potential of 33 ± 1 mV (Fig. 3A and B). These values were comparable to those of ZIF-8 nanomaterials without encapsulated CA4, which exhibited a hydrodynamic diameter of 132 ± 4 nm (Fig. 3A) and a zeta potential of 33 ± 2 mV (Fig. 3B). Considering that PIC carries a negative charge due to its RNA characteristics, we prepared PIC/CA4@ZIF-8 nanomaterials using an electrostatic adsorption method, where PIC was loaded into the CA4@ZIF-8 nanomaterials. We investigated different mass ratios between ZIF-8 and PIC and found that a mass ratio of 200 : 1 resulted in complete complexation (Fig. 3C). Subsequently, PIC/CA4@ZIF-8 was synthesized using this mass ratio, and the resulting nanomaterials exhibited a hydrodynamic diameter of approximately 2734 ± 91 nm (Fig. 3A) and a zeta potential of 21 ± 2 mV (Fig. 3B). The decrease in zeta potential compared to CA4@ZIF-8 indicated the successful incorporation of PIC into the nanomaterials. Furthermore, SEM analysis revealed a uniform spherical structure of PIC/CA4@ZIF-8 nanomaterials with an average particle size of approximately 800 nm (Fig. 3D). RNA protection experiments demonstrated that when PIC and PIC@ZIF-8 were co-incubated with equal amounts of RNAase, degradation of PIC into smaller RNA fragments was observed over time (Fig. 3E). In contrast, PIC@ZIF-8 exhibited effective protection, with complete degradation occurring after 12 hours, compared to within 3 hours for free PIC. These results indicate that ZIF-8 effectively

protects PIC from RNAase degradation and significantly prolongs its shelf life.

Subsequently, we combined PIC/CA4@ZIF-8 with HA hydrogel to form PIC/CA4@ZIF-8/HA Gel. FTIR analysis confirmed the successful conversion of carboxyl groups in HA-CHO, as evidenced by a prominent absorption peak at 1730 cm^{-1} (Fig. 3F). Next, HA-CHO was crosslinked with ADH to form HA hydrogel (HA Gel) (Fig. 3G). The combination of HA-CHO, PIC/CA4@ZIF-8, and ADH resulted in the formation of a novel composite hydrogel, namely PIC/CA4@ZIF-8/HA Gel (Fig. 3G). Dynamic frequency sweep analysis was performed to evaluate the mechanical properties of the hydrogels. The storage modulus (G') of the PIC/CA4@ZIF-8/HA gel group was approximately ten times higher than the loss modulus (G'') compared to the HA gel group (Fig. 3H), indicating significantly improved stability of PIC/CA4@ZIF-8/HA gel. Additionally, the injectability of PIC/CA4@ZIF-8/HA gel was confirmed through a syringeability test (Fig. 3I), demonstrating its potential for *in situ* injection. SEM images revealed a porous structure of both the HA and PIC/CA4@ZIF-8/HA gels (Fig. 3J). Notably, the PIC/CA4@ZIF-8/HA gel group exhibited elevated structures on the surface, attributed to the attachment of PIC/CA4@ZIF-8 nanomaterials to the hydrogel. These results demonstrate that we successfully synthesized an injectable hydrogel, PIC/CA4@ZIF-8/HA, which is able to co-deliver CA4 and PIC.

3.4. PIC/CA4@ZIF-8/HA exhibits a more pronounced therapeutic effect in melanoma

We conducted further investigations to assess the sustained *in vivo* release effect of the hydrogel. The results depicted in Fig. 4A demonstrate a significantly prolonged presence of fluorescence in mouse tumor tissues when ICG was incorporated within ZIF-8/HA. This effect persisted for up to 7 days longer compared to ICG encapsulated solely in ZIF-8 (which disappeared by day 5) and free ICG (which almost disappeared by day 3). These findings indicate the superior long-term drug release capabilities of our ZIF-8/HA formulation. To evaluate the therapeutic effectiveness of PIC/CA4, PIC/CA4@ZIF-8, and PIC/CA4@ZIF-8/HA formulations, we employed a subcutaneous tumor mouse model. Considering the optimal loading capacity of ZIF-8/HA, we administered CA4 at a dosage of 1 mg kg^{-1} and PIC at 0.05 mg kg^{-1} for each group in a single administration (Fig. 4B). Remarkably, even at these low doses of CA4 and PIC (1/10 of the previous single-dose for CA4 and only 1/20 of the previous single-dose for PIC), administered only once, the PIC/CA4 combination still exhibited significant anti-tumor effects (Fig. 4C and D). This suggests a synergistic interaction between PIC and CA4 for melanoma suppression. In comparison, the PIC/CA4@ZIF-8/HA formulation demonstrated even more pronounced inhibition of tumor growth, indicating superior therapeutic efficacy compared to co-administration of PIC/CA4. Despite the significant reduction in tumor volume in mice treated with PIC/CA4, histological analysis using H&E staining (Fig. 4E) and immunofluorescence experiments (Fig. 5A) revealed the presence of abundant vascular-like structures in the tumor tissues of the PIC/CA4-treated group. This finding suggests that over time, the injected PIC and CA4 gradually degrade, leading to a loss of their effects on vascular disruption in the tumor tissue, which may result in tumor recurrence. In contrast, the PIC/CA4@ZIF-8/HA treatment group exhibited barely visible vascular-like structures within the tumor tissue (Fig. 5A), accompanied by a significant infiltration of immune cells (Fig. 4E), particularly M1 macrophages (Fig. 5C). Although significant macrophage infiltration can also be observed in other groups (Fig. 5B), it is evident that very few M1 macrophages are present (Fig. 5C). These findings highlight the enhanced therapeutic efficacy of the hydrogel-encapsulated PIC/CA4@ZIF-8, which prolongs the retention time of both PIC and CA4, thereby promoting potential anti-angiogenic

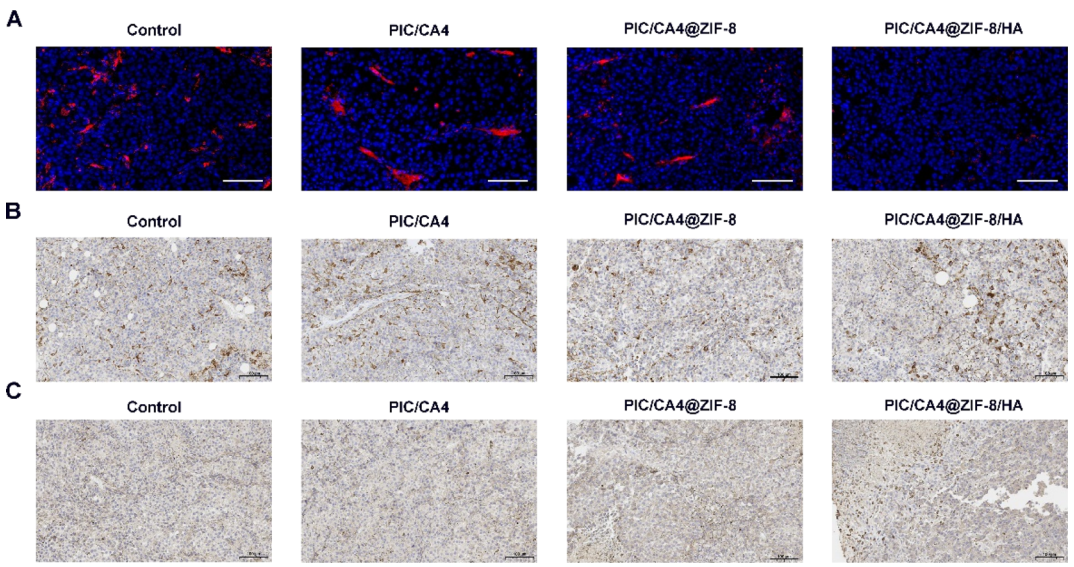

Fig. 5 PIC/CA4@ZIF-8/HA disrupts angiogenesis and promotes M1 macrophage infiltration in tumor tissue. (A) Representative images of tumor vessel density in tumor tissues. Scale bar, 100 μm. (B) Immunohistochemical staining of F4/80 expression in mouse tumor tissue. Scale bar, 100 μm. (C) Immunohistochemical staining of CD86 expression in mouse tumor tissue. Scale bar, 100 μm.

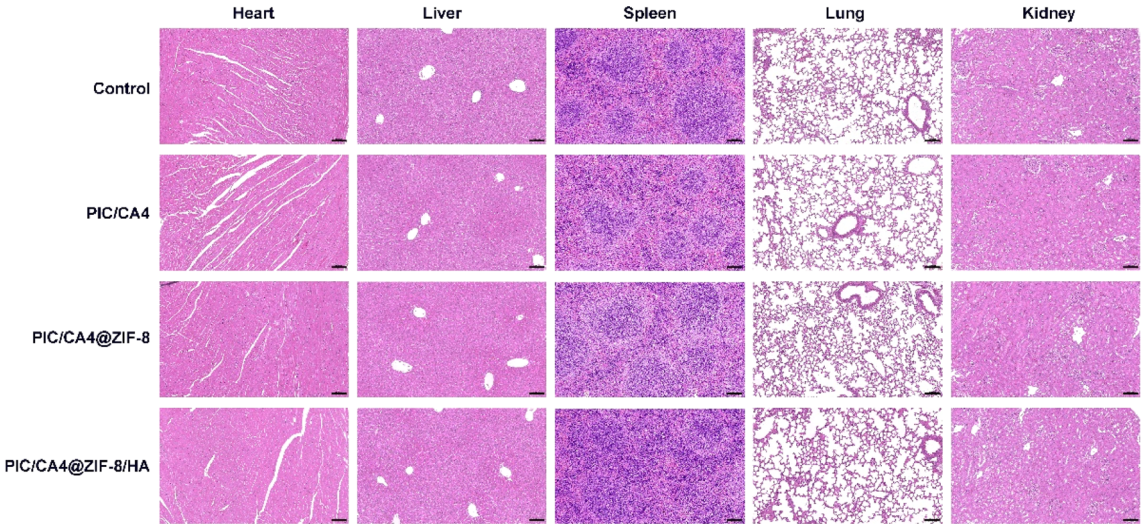

Fig. 6 *In vivo* safety assessment of mouse treated with PBS, PIC/CA4, PIC/CA4@ZIF-8, and PIC/CA4@ZIF-8/HA. H&E staining images of heart, liver, spleen, lung, and kidney. Scale bar, 100 μm.

immune activation. Furthermore, it is important to note that co-delivery of PIC and CA4 using ZIF-8 nanoparticles did not yield as favorable outcomes as simultaneous administration of PIC and CA4. This discrepancy can be attributed to multiple factors, including the enhanced augmentation of angiogenesis (as illustrated in Fig. 4E and 5A). Further investigation is necessary to elucidate the precise causes.

3.5. PIC/CA4@ZIF-8/HA exhibits excellent biosafety *in vivo*

To evaluate the biosafety of the various treatment modalities, we collected heart, liver, spleen, lung, and kidney tissues from both the tumor control group and the mice treated with different therapies. Paraffin sections were prepared from these tissues and subjected to H&E staining. The results, presented in Fig. 6, demonstrate that the heart, liver, spleen, lung, and kidney tissues of mice treated with different therapies maintained their structural integrity. In the heart tissues, the cardiac myocytes displayed a regular arrangement, and no infiltration of inflammatory cells was observed. The hepatocytes in the liver tissue exhibited uniform size and arrangement, with well-preserved liver lobules and clearly defined boundaries. The spleen tissues exhibited well-structured white pulp and red pulp with distinct boundaries and homogeneous distribution. The lung tissues displayed no noticeable alterations in lung cells, and the alveolar structure remained intact and uniform. The renal glomeruli exhibited a normal morphology without any significant infiltration of inflammatory cells. These findings indicate that the different treatment modalities demonstrated a certain degree of biological safety, with no significant toxic side effects observed in the organs and tissues of the mice. Thus, they can be considered safe for melanoma treatment.

4. Conclusions

In conclusion, we have successfully developed a novel anti-angiogenic immunotherapy approach for suppressing melanoma. Our study demonstrates the remarkable anti-tumor efficacy of the PIC/CA4 combination in inhibiting melanoma growth, particularly when delivered using the PIC/CA4@ZIF-8/HA formulation, without compromising biosafety. These findings highlight the synergistic effects of PIC and CA4, and underscore the potential of ZIF-8/HA as a targeted and enhanced therapeutic carrier. This therapeutic strategy holds significant promise as an alternative treatment option for melanoma.

Author contributions

Jiaojiao Zhao: conceptualization, methodology, investigation, data curation, formal analysis, project administration, funding acquisition, writing-original draft, writing-review & editing. Zhengkui Zhang: conceptualization, methodology, investigation, project administration, funding acquisition, data curation, writing-original draft. Xufeng Xiao: methodology, data curation, investigation, funding acquisition, writing-original draft. Yunuo Zheng: methodology, data curation, investigation, writing-original draft. Tianlong Wang: methodology, data curation, writing-original draft. Xiaoqing Zhang: methodology, data curation, visualization, writing-original draft. Gaochuan Fang: methodology, investigation, data curation, writing-original draft. Zhonghai Zhang: methodology, investigation, data curation, writing-original draft.

Conflicts of interest

There are no conflicts of interest to declare.

Acknowledgements

This work was supported by the Natural Science Foundation of Xuzhou City (KC22025), the Natural Science Foundation of the Jiangsu Higher Education Institutions of China (23KJB180009), the High-level Innovation and Entrepreneurship Talent

Introduction Program of Jiangsu Province of China (JSSCBS20211269), the Natural Science Foundation of Jiangsu Province (BK20220673), the Postgraduate Research and Practice Innovation Program of Jiangsu Province (KYCX22_2801), and the Priority Academic Program Development of Jiangsu Higher Education Institutions (PAPD).

References

1 G. V. Long, S. M. Swetter, A. M. Menzies, J. E. Gershenwald and R. A. Scolyer, *Lancet*, 2023, **402**, 485–502.
2 J. Timar and A. Ladanyi, *Int. J. Mol. Sci.*, 2022, **23**, 5384.
3 K. Eddy and S. Chen, *Int. J. Mol. Sci.*, 2020, **21**, 8984.
4 M. S. Carlino, J. Larkin and G. V. Long, *Lancet*, 2021, **398**, 1002–1014.
5 S. Zhu, T. Zhang, L. Zheng, H. Liu, W. Song, D. Liu, Z. Li and C. X. Pan, *J. Hematol. Oncol.*, 2021, **14**, 156.
6 N. Kumari and S. H. Choi, *J. Exp. Clin. Cancer Res.*, 2022, **41**, 68.
7 A. J. Boutilier and S. F. Elsawa, *Int. J. Mol. Sci.*, 2021, **22**, 6995.
8 M. Roh-Johnson, A. N. Shah, J. A. Stonick, K. R. Poudel, J. Kargl, G. H. Yang, J. di Martino, R. E. Hernandez, C. E. Gast, L. R. Zarour, S. Antoku, A. M. Houghton, J. J. Bravo-Cordero, M. H. Wong, J. Condeelis and C. B. Moens, *Dev. Cell*, 2017, **43**, 549–562.
9 F. H. Barnett, M. Rosenfeld, M. Wood, W. B. Kiosses, Y. Usui, V. Marchetti, E. Aguilar and M. Friedlander, *Sci. Rep.*, 2016, **6**, 36659.
10 O. E. Rahma and F. S. Hodi, *Clin. Cancer Res.*, 2019, **25**, 5449–5457.
11 J. Tu, H. Liang, C. Li, Y. Huang, Z. Wang, X. Chen and X. Yuan, *Front. Immunol.*, 2023, **14**, 1198972.
12 A. Mantovani, P. Allavena, F. Marchesi and C. Garlanda, *Nat. Rev. Drug Discovery*, 2022, **21**, 799–820.
13 Y. Zheng, B. Jiang, H. Guo, Z. Zhang, B. Chen, Z. Zhang, S. Wu and J. Zhao, *Nanomedicine*, 2023, **49**, 102658.
14 C. Montemagno and G. Pages, *Front. Cell Dev. Biol.*, 2020, **8**, 584.
15 R. Smolarczyk, J. Czapla, M. Jarosz-Biej, K. Czerwinski and T. Cichon, *Eur. J. Pharmacol.*, 2021, **891**, 173692.
16 Z. R. Huinen, E. J. M. Huijbers, J. R. van Beijnum, P. Nowak-Sliwinska and A. W. Griffioen, *Nat. Rev. Clin. Oncol.*, 2021, **18**, 527–540.
17 Y. Fang, X. Luo, Y. Xu, Z. Liu, R. L. Mintz, H. Yu, X. Yu, K. Li, E. Ju, H. Wang, Z. Tang, Y. Tao and M. Li, *Adv. Sci.*, 2023, **10**, e2300899.
18 T. G. Dacoba, C. Anfray, F. Mainini, P. Allavena, M. J. Alonso, F. Torres Andon and J. Crecente-Campo, *Front. Immunol.*, 2020, **11**, 1412.
19 J. Zhao, Z. Zhang, Y. Xue, G. Wang, Y. Cheng, Y. Pan, S. Zhao and Y. Hou, *Theranostics*, 2018, **8**, 6307–6321.
20 C. Anfray, F. Mainini, E. Digifico, A. Maeda, M. Sironi, M. Erreni, A. Anselmo, A. Ummarino, S. Gandoy, F. Exposito, M. Redrado, D. Serrano, A. Calvo, M. Martens, S. Bravo, A. Mantovani, P. Allavena and F. T. Andon, *J. Immunother. Cancer*, 2021, **9**, e002408.
21 K. Guo, X. Ma, J. Li, C. Zhang and L. Wu, *Eur. J. Med. Chem.*, 2022, **241**, 114660.
22 G. J. Rustin, S. M. Galbraith, H. Anderson, M. Stratford, L. K. Folkes, L. Sena, L. Gumbrell and P. M. Price, *J. Clin. Oncol.*, 2003, **21**, 2815–2822.
23 A. F. Welford, D. Biziato, S. B. Coffelt, S. Nucera, M. Fisher, F. Pucci, C. Di Serio, L. Naldini, M. De Palma, G. M. Tozer and C. E. Lewis, *J. Clin. Invest.*, 2011, **121**, 1969–1973.
24 H. D. Lawson, S. P. Walton and C. Chan, *ACS Appl. Mater. Interfaces*, 2021, **13**, 7004–7020.
25 A. K. Bindra, D. Wang and Y. Zhao, *Adv. Mater.*, 2023, **35**, e2300700.
26 J. Y. C. Lim, L. Goh, K. I. Otake, S. S. Goh, X. J. Loh and S. Kitagawa, *Biomater. Sci.*, 2023, **11**, 2661–2677.
27 H. N. Abdelhamid, *Curr. Med. Chem.*, 2021, **28**, 7023–7075.
28 Y. Wang, H. Wang, Y. Song, M. Lv, Y. Mao, H. Song, Y. Wang, G. Nie, X. Liu, J. Cui and X. Zou, *J. Nanobiotechnol.*, 2022, **20**, 96.
29 J. Feng, W. Yu, Z. Xu, J. Hu, J. Liu and F. Wang, *ACS Appl. Mater. Interfaces*, 2020, **12**, 22613–22623.
30 M. Pourmadadi, A. Aslani and M. Abdouss, *Int. J. Biol. Macromol.*, 2023, **243**, 125168.
31 Y. Liu, T. Li, M. Sun, Z. Cheng, W. Jia, K. Jiao, S. Wang, K. Jiang, Y. Yang, Z. Dai, L. Liu, G. Liu and Y. Luo, *Acta Biomater.*, 2022, **146**, 37–48.
32 S. S. Soni, A. M. D'Elia, A. Alsasa, S. Cho, T. Tylek, E. M. O'Brien, R. Whitaker, K. L. Spiller and C. B. Rodell, *Biomater. Sci.*, 2022, **10**, 6951–6967.
33 H. Wang, X. Li, B. W. Tse, H. Yang, C. A. Thorling, Y. Liu, M. Touraud, J. B. Chouane, X. Liu, M. S. Roberts and X. Liang, *Theranostics*, 2018, **8**, 1227–1242.
34 M. E. Nik, A. A. Momtazi-Borojeni, P. Zamani, J. G. Navashenaq, M. Iranshahi, M. R. Jaafari and B. Malaekeh-Nikouei, *J. Cell. Physiol.*, 2019, **234**, 14721–14733.
35 Y. Wang, L. Dong, H. Zhong, L. Yang, Q. Li, C. Su, W. Gu and Y. Qian, *Int. J. Biol. Sci.*, 2019, **15**, 2110–2118.
36 I. Nasir, C. McGuinness, A. R. Poh, M. Ernst, P. K. Darcy and K. L. Britt, *Trends Immunol.*, 2023, **44**, 971–985.
37 S. Chen, A. Saeed, Q. Liu, Q. Jiang, H. Xu, G. G. Xiao, L. Rao and Y. Duo, *Signal Transduction Targeted Ther.*, 2023, **8**, 207.